New insights into the humic acid fouling mechanism of ultrafiltration membranes for different Ca^{2+} dosage ranges: results from micro- and macro-level analyses

Rui Miao, Ying Wu, Pei Wang, Gongzheng Wu, Lei Wang, Xingfei Li, Jiaxuan Wang, Yongtao Lv and Tingting Liu

ABSTRACT

To reveal the mechanisms of the influence of Ca^{2+} on membrane fouling with humic acid (HA), the adhesion forces of HA with both other HA molecules and the membrane, the HA fouling layer structure, HA fouling experiments, and the HA rejections at a wide range of Ca^{2+} dosages were investigated. The results indicated that the effect of Ca^{2+} on HA fouling can be divided into three stages. At lower ionic strength (IS) of $CaCl_2$, the change in electrostatic forces is the main factor in controlling HA fouling behavior; i.e., increasing Ca^{2+} dosages resulted in more serious membrane fouling. When the IS of $CaCl_2$ reached 10 mM, HA aggregates became the dominant factor in the fouling process, which could result in a porous fouling layer accompanied by less membrane fouling. Interestingly, much weaker membrane fouling was observed when the IS increased to 100 mM and the HA rejection began to decline. This was because a stronger hydration repulsion force was generated, which could weaken the compactness of the fouling layer and the adhesion forces of HA with both the membrane and HA, while enabling smaller-sized HA to pass more easily into the permeate, which led to less membrane fouling and a lower HA rejection.

Key words | aggregates, Ca^{2+}, electrostatic forces, humic acid fouling, hydration repulsion forces, ultrafiltration membranes

Rui Miao
Ying Wu
Pei Wang
Gongzheng Wu
Lei Wang (corresponding author)
Xingfei Li
Jiaxuan Wang
Yongtao Lv
Tingting Liu
Key Laboratory of Membrane Separation of Shaanxi Province,
Xi'an University of Architecture and Technology,
Xi'an 710055,
China
E-mail: *wl0178@126.com*

Rui Miao
Lei Wang
Yongtao Lv
Research Institute of Membrane Separation Technology of Shaanxi Province,
Xi'an 710055,
China

INTRODUCTION

Humic acid (HA) is the main compound of natural organic matter, which exists widely in surface water, municipal wastewater, seawater, and other aquatic environments. HA is also a widely known precursor to potentially carcinogenic disinfection byproducts (Kyzas *et al.* 2017); therefore, removing HA from water or wastewater is a widespread concern. Ultrafiltration (UF) technology is one of the effective technologies for separating HA foulants from water sources (Szymański *et al.* 2016). However, HA fouling of membranes causes a rapid and irreversible loss of flux through the membrane, which is one of the major limiting factors for the successful application of UF technology in water or wastewater treatment (Shankar *et al.* 2017).

Many factors influence HA fouling of membranes, such as feedwater solution chemistry, membrane properties, and hydrodynamic and operating conditions (Lin *et al.* 2015). Among them, the most typical and widespread divalent ion in waters and wastewaters (such as natural waters, municipal wastewater, and seawater), i.e., the Ca^{2+} ion, has been widely reported to be a crucial factor that could seriously affect the HA fouling behavior in membranes (Wang *et al.* 2015). The functional groups in HA molecules easily interact with Ca^{2+} via electrical double layers, neutralization, or complexation, which can significantly influence the HA fouling layer structure and the deposition behavior of HA onto the membrane surface, which then will affect the fouling potential (Sutzkover-Gutman *et al.* 2010). Therefore, unraveling the mechanisms of the effect of Ca^{2+} on HA fouling behavior in membranes has continued to be of interest.

Some previous studies have reported the effects of Ca^{2+} on membrane fouling with HA; however, the influence of Ca^{2+} on membrane fouling with HA is still unclear and some contradictory findings were obtained.

doi: 10.2166/wst.2018.141

For the most part, the HA fouling rate and extent have been exacerbated in the presence of divalent Ca^{2+} (Tang *et al.* 2007; Tian *et al.* 2013; Lin *et al.* 2015). Most researchers believe that with the increase in Ca^{2+} concentrations, more Ca^{2+} crosslinking or bridging interactions occur between HA molecules or between the membrane surface and HA, which could cause a more compacted gel network in the fouling layer and a rapid deposition of HA onto the membrane surface. This eventually leads to the phenomenon of more serious membrane fouling in the presence of Ca^{2+} (Sutzkover-Gutman *et al.* 2010; Tian *et al.* 2013).

However, several other research groups investigating the effects of Ca^{2+} on membrane fouling with HA found that HA fouling rate/extent decreased visibly at some Ca^{2+} concentrations, which is contrary to the findings mentioned above (Katsoufidou *et al.* 2005; Nghiem *et al.* 2006; Katsoufidou *et al.* 2008; Nghiem *et al.* 2008; Shao *et al.* 2011). Until now, however, the reason for reduced membrane fouling with Ca^{2+} has still been unclear and only tentative explanations have been given. For example, Shao *et al.* speculated that the complexation/bridging interactions between HA molecules are enhanced with the increase in Ca^{2+} dosage, which led to the formation of large aggregates. These large HA aggregates are retained on the membrane surface, which results in a more porous fouling layer with a comparatively higher permeability. Consequently, the membrane fouling rate/extent began to decrease (Shao *et al.* 2011). However, Nghiem *et al.* found that although membrane fouling decreased at higher Ca^{2+} dosages, the foulant rejection also decreased. This result appears not to support the speculation that larger HA aggregates are formed at higher Ca^{2+} dosages. Nghiem *et al.* did not present any further discussion or pursue any further studies to find the cause of this phenomenon (Nghiem *et al.* 2006, 2008).

The studies mentioned above indicate that two kinds of opposing results about the effects of Ca^{2+} on HA fouling behavior have been demonstrated to date. However, it appears that no study has focused on identifying the reason for the different characteristics with Ca^{2+} shown in membrane fouling with HA, and particularly the reason for the enhancement or mitigation mechanisms of Ca^{2+} on membrane fouling are still unclear or debatable. Most existing explanations appear to be simple descriptions or speculation based on experimental observations (Singh & Song 2005). Therefore, more research is needed into the effect of different Ca^{2+} dosages on membrane fouling with HA, which may be helpful in resolving the above issues and also effectively explain the different characteristics observed while using Ca^{2+} in membrane fouling with HA.

In the present work, polyvinylidene fluoride (PVDF) UF membranes were used to filter HA solutions for a wide range of Ca^{2+} dosages. Atomic force microscopy (AFM) associated with specific colloidal probes was used to determine the adhesion forces of HA with both HA and PVDF membrane at corresponding Ca^{2+} dosages. A quartz crystal microbalance with dissipation monitoring (QCM-D) was used to investigated the influences of different Ca^{2+} dosages on the HA fouling layer structure. These results were combined with the HA rejection and the hydrodynamic diameter of HA at corresponding Ca^{2+} dosages to give a better explanation for the HA fouling mechanism at different Ca^{2+} concentrations.

MATERIALS AND METHODS

Humic acids and membrane preparation

HA was purchased from Sigma-Aldrich (St Louis, MO, USA), and stock HA (1 g/L) solution was prepared. The fresh HA working solution was prepared before each HA filtration experiment and maintained at a pH of 7.0 and a dissolved organic carbon (DOC) concentration of 10 mg/L. Throughout this work, 0.01 mol/L NaOH or 0.01 HCl mol/L solutions were used to adjust the pH values of the HA working solutions as needed, and 0.5 mol/L $CaCl_2$ stock solution was used to adjust the ionic strength (IS) of the HA working solutions. The IS of $CaCl_2$ of the HA working solution was set at 0, 1, 10, and 100 mM. These values were selected because the range of 0–1 mM represents very soft water or wastewater, while 10 mM corresponds to 'hard' water and 100 mM would be encountered in special water or wastewater feed, such as seawater and brine or in chemical cleaning. Moreover, unless otherwise stated, all reagents and chemicals were analytical reagents with a purity exceeding 99% and ultrapure water was used to prepare all working solutions.

The present work used flat-sheet PVDF UF membranes that were synthesized in the laboratory by a phase inversion method. PVDF and *N*, *N*-dimethylacetamide were the predominant materials for the preparation of membranes, which were purchased from Solvay Advanced Polymers Co. (Solef 1015; USA) and Tianjin Fucheng Chemical Reagent Co. (Tianjin, China), respectively. The preparation procedure and characteristics of PVDF UF membranes were described in detail previously (Miao *et al.* 2017); the pure water flux, surface roughness, and contact angle of the membranes were 300 ± 20 L/(m^2·h), 17.5 nm, and $75 \pm 2°$, respectively.

HA filtration and flux recovery tests

As previously reported (Miao *et al.* 2017), a stirred dead-end filtration system was used in all HA filtration experiments with PVDF UF membranes. The effective filtration area of membranes was $3.32 \times 10^{-3}\ m^2$ and the constant pressure of the filtration system was provided by a compressed nitrogen gas cylinder. During the filtration experiments, a computer connected to an electronic balance recorded the permeate flux (J) data of the corresponding tested membrane continuously. Unless otherwise noted, a new PVDF membrane was used in each filtration experiment. The HA filtration experiment procedure was as described in the following paragraphs.

First, a clean PVDF membrane was compacted at pressure of 0.15 MPa until the permeate flux stabilized. The pure water flux (J_0) of the membrane was then measured at pressure of 0.10 MPa. And finally, at pressure of 0.10 MPa, the HA feed solution was filtered with the desired IS of $CaCl_2$ for 120 min. The permeate flux of the membrane at this stage was recorded continuously and J/J_0 was used to evaluate the flux decline behavior in PVDF membranes for convenient comparison. The fouling experiments were repeated at least six times for each IS condition of $CaCl_2$.

After the corresponding filtration test, a physical cleaning process was carried out on the HA-fouled membrane: the HA-fouled membrane was put into a 400 mL deionized water in a beaker, which was then placed in a multivibrator and vibrated for 2 min. Finally, the permeate flux (J_r) of the cleaned membrane was determined at pressures of 0.10 MPa and cleaning efficiency was evaluated by the flux recovery rate (J_r/J_0).

The HA rejection (R) of the PVDF membranes for different IS of $CaCl_2$ was measured as:

$$R = \left(1 - \frac{C_p}{C_f}\right) \times 100\%$$

where C_p is the DOC concentration of the HA permeate and C_f is the DOC concentration of the corresponding HA feed solution. The filtration times at which the HA rejections were measured were identical.

Adhesion force measurements

First, carboxyl colloidal probes were developed by our research group because HA is rich in carboxyl groups. The preparation method of the carboxyl-group probe was followed as detailed previously (Miao *et al.* 2015). The carboxyl colloidal probes were used as HA surrogates and associated with a MultiMode 8.0 AFM (Bruker, Germany) to determine the adhesion forces of HA with both HA and PVDF membranes at different IS of $CaCl_2$.

All measurements of adhesion forces were performed in a fluid cell under contact mode. In measuring the adhesion force of HA with both HA and PVDF membranes, the test samples were an HA-fouled membrane and a clean PVDF membrane, respectively. The HA solution that was used in the corresponding filtration experiments was used as a test solution for HA–HA adhesion forces and an aqueous solution with desired IS of $CaCl_2$ was used as a test solution for PVDF membrane–HA adhesion forces. To minimize the intrinsic error resulting in part from membrane surface heterogeneity, the adhesion force under the desired IS of $CaCl_2$ was determined at six different locations. At least 15 force curves were achieved for each site. In addition, the integrity of all used carboxyl probes was checked by a scanning electron microscope to ensure the precision of the adhesion force measurements.

QCM-D experiments

A QCM-D system (E1; Qsence, Sweden) was used to investigate the structure of the HA fouling layers at different Ca^{2+} dosages. Before each QCM-D experiment, a PVDF-coated sensor crystal was developed and thoroughly cleaned using the preparation method and process described previously (Miao *et al.* 2017).

In the QCM-D experiments, the flow module of the system was equipped with a clean PVDF-coated sensor crystal. This system was then pre-equilibrated with ultrapure water to achieve a stable baseline. Finally, the HA feed solution with the targeted Ca^{2+} dosage was pumped into the system for 25 min. During this stage, increase in dissipation (ΔD) and decrease in frequency (Δf) from the baseline were monitored continuously.

The $|\Delta D/\Delta f|$ ratio, i.e., the energy dissipation value per unit adsorbed mass change, provides information about the HA fouling layer structure at the corresponding Ca^{2+} concentration. That is, a higher $|\Delta D/\Delta f|$ ratio suggests the formation of a relatively nonrigid and looser HA fouling layer structure, whereas a lower $|\Delta D/\Delta f|$ ratio indicates a denser HA fouling layer (Chang & Bouchard 2013).

All QCM-D experiments were conducted at 23 °C. To maintain laminar flow in the module, the flow rate through the measurement chamber was kept at 0.1 mL/min. Both Δf and ΔD at the third overtone were used. Each QCM-D measurement was carried out at least three times.

Analyses

At various ISs of $CaCl_2$, the zeta potentials and hydrodynamic diameters of HA were measured with a Zetasizer Nano instrument (ZS90; Malvern Instruments, Malvern, UK). The zeta potentials of PVDF membranes were quantified with an electrokinetic analyzer for solid surface analysis (SurPASS; Anton Paar GmbH, Graz, Austria). A total organic carbon analyzer (CPN; Shimadzu, Kyoto, Japan) was employed to measure the DOC concentrations of HA feed solutions or permeate.

RESULTS AND DISCUSSION

Charge characteristics of PVDF membranes and HA at different Ca^{2+} concentrations

The charge characteristics of the PVDF membrane and HA molecules are closely correlated with the electrostatic interaction forces of HA with both HA and membrane, which may be easily affected by the Ca^{2+} concentration (Yamamura *et al.* 2008). Therefore, the zeta potentials of PVDF membranes and HA at IS of 0, 1, 10, and 100 mM $CaCl_2$ were determined systematically and are summarized in Table 1.

As shown in Table 1, the HA molecules and PVDF membrane were negatively charged at all IS of $CaCl_2$ investigated, which indicates that the electrostatic force of HA with both HA and PVDF membrane were repulsion forces. Furthermore, with increasing IS of $CaCl_2$, the zeta potentials of both the HA molecules and the membrane decreased significantly, which was mainly because the charge neutralization, compression of the electrical double layer, and bridging action or complexation of Ca^{2+} were strengthened (Shen *et al.* 2011). This should also indicate that the electrostatic repulsion forces of HA with both PVDF and HA decreased with increasing Ca^{2+} dosage.

Influences of Ca^{2+} concentrations on the macro membrane fouling with HA

HA filtration tests were carried out at IS of 0, 1, 10, and 100 mM $CaCl_2$, respectively. The normalized flux decline curves and the flux recovery efficiency of HA-fouled membranes at corresponding Ca^{2+} dosages are presented in Figures 1 and 2, respectively. As is clearly shown in the figures, with the increase of Ca^{2+} dosages, the variation trend in the flux decline rate and the flux recovery rate can be divided into two stages.

First, when increasing the IS from 0 to 1 mM, the extent of flux decline increased sharply from 33% to 77%, and the flux recovery rate decreased from 98% to 27%. Clearly, the membrane fouling rate and irreversible fouling were exacerbated significantly with the addition of a Ca^{2+} ion. This is in accordance with the results of most previous investigations (Seidel & Elimelech 2002; Tang *et al.* 2007; Tian *et al.* 2013). These studies suggested that the electrostatic repulsive force of HA with both HA and PVDF membrane would decrease with the addition of a Ca^{2+} ion, which could result in a denser HA fouling layer and much more serious membrane fouling.

In contrast, when the IS of $CaCl_2$ exceeded 1 mM, the flux decline rate and irreversible fouling extent began to decrease with increasing Ca^{2+} dosage. In particular, when the IS reached 100 mM, the flux of HA-fouled membranes

Table 1 | Zeta potentials of PVDF membranes and HA surface at various Ca^{2+} dosages

IS (mM)		0	1	10	100
Zeta potential (mV)	PVDF membrane	−29.7	−11.9	−5.5	−4.3
	HA	−46.7	−19.7	−13.6	−8.3

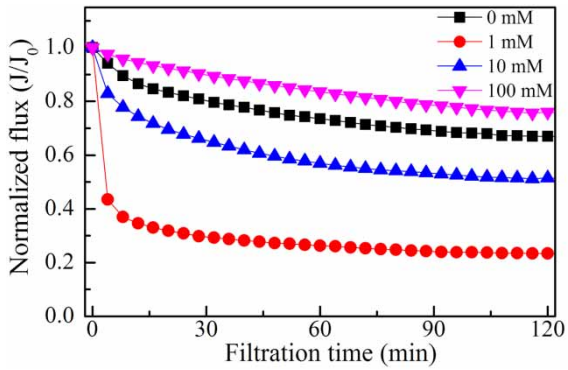

Figure 1 | Normalized flux with filtration time of HA-fouled membranes at different Ca^{2+} dosages.

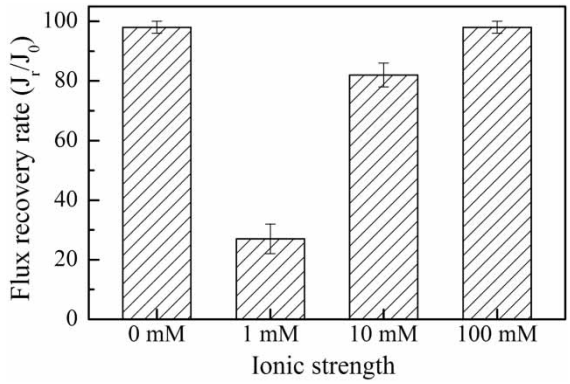

Figure 2 | The flux recovery rate of HA-fouled membranes at different Ca^{2+} dosages.

only declined by 24%; meanwhile the flux was almost fully recovered after cleaning. Similar phenomena have also been reported by Shao *et al.* (2011) and Katsoufidou *et al.* (2008), who investigated the HA fouling behavior of UF membranes at different Ca^{2+} dosages. They suggested that, with increasing Ca^{2+} concentrations, the complexation/bridging interactions of HA with both membrane and HA were gradually enhanced, which thus promoted the formation of larger HA aggregates. Such larger HA aggregates apparently tended to form looser and more porous HA fouling with relatively high permeability, which then resulted in less membrane fouling. However, as shown in Figure 3, the HA rejections of the PVDF membrane decreased significantly at IS of 100 mM $CaCl_2$. This observation appeared to contrast somewhat with the above speculation that larger HA aggregates form at higher Ca^{2+} dosages because, compared with the relatively smaller HA molecules, the larger HA aggregates are more easily retained on the membrane surface (Yuan & Zydney 1999).

Based on the above discussion, it is clear that membrane fouling was enhanced with Ca^{2+} at relatively lower IS. In contrast, when the Ca^{2+} dosage exceeded a critical value, membrane fouling began to decline with increasing Ca^{2+} dosages. This phenomenon appears to suggest that the influence of Ca^{2+} on the HA fouling of membranes is different at different Ca^{2+} dosages. However, few researchers seem to have conducted insightful and systematic studies to unravel the reasons for the 'different influence behavior'. Therefore, further studies are required.

Influences of Ca^{2+} concentrations on the adhesion forces of HA with both HA and PVDF

At IS of 0, 1, 10, and 100 mM $CaCl_2$, the adhesion forces of HA with both HA and PVDF membrane were measured systematically. The corresponding representative adhesion force curves are presented in Figure 4.

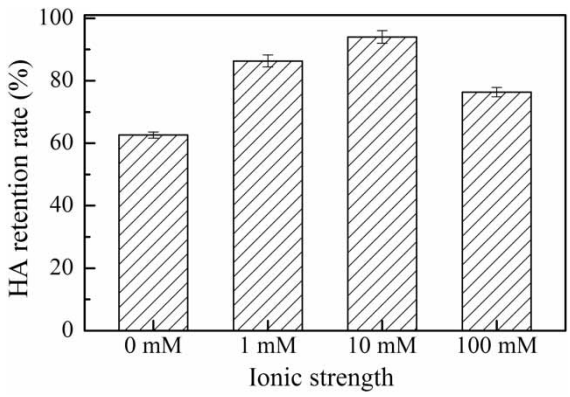

Figure 3 | The HA rejections of a PVDF membrane at different IS of $CaCl_2$.

It is clear that, with increasing Ca^{2+} dosages, the variation trend of the adhesion forces of HA with both HA and PVDF membrane was divided into two stages, which is similar to the variation in the characteristics of the flux decline and recovery rate/extent of corresponding HA-fouled membranes (as shown in Figures 1 and 2).

At IS of 0, 1, and 10 mM $CaCl_2$, the average adhesion forces of HA with PVDF membrane were 6.6 ± 0.38, 7.5 ± 0.57, and 9.6 ± 0.76 mN/m, respectively, and the average adhesion forces of HA with HA were 0.50 ± 0.03, 1.71 ± 0.11, and 2.15 ± 0.18 mN/m, respectively. Clearly, in the IS of 0–10 mM $CaCl_2$, the adhesion forces of HA with both HA and PVDF membrane increased gradually with increasing Ca^{2+} dosages. This was mainly because the complexation/bridging actions, neutralization, or charge screening were strengthened by increasing the Ca^{2+} dosage, which reduced the net charges of the HA molecules and the membrane. This reduction of net charges led to a decrease in the electrostatic repulsion forces of HA with both HA and membrane, eventually leading to the corresponding adhesion forces increasing with increasing Ca^{2+} dosages (Mo *et al.* 2008).

While increasing the IS from 10 to 100 mM, the average PVDF–HA adhesion force decreased sharply from 9.6 ± 0.76 to 2 ± 0.12 mN/m and the HA–HA adhesion force decreased from 2.15 ± 0.18 to 0.52 ± 0.04 mN/m. It is interesting to note that in this range of IS, the adhesion forces of HA with both HA and PVDF membrane began to decline with increasing Ca^{2+} dosages, although the electrostatic repulsion forces of HA with both HA and PVDF membrane still decreased with increasing Ca^{2+} dosages (as discussed in section 'Charge characteristics of PVDF membranes and HA at different Ca^{2+} concentrations'). This phenomenon is contrary to the observations at IS of 0–10 mM $CaCl_2$, which may be explained effectively by the balance of electrostatic interaction forces and hydration repulsion forces.

As mentioned above, the electrostatic repulsion forces of HA with both HA and PVDF membrane decreased with an increase in Ca^{2+} dosage. Simultaneously, because Ca^{2+} is one of the most typical hydrated ions, the hydration repulsion forces of HA with both HA and PVDF membrane would be provoked and increase with an increase in Ca^{2+} dosage, which is a relatively short-range repulsive force and difficult to distinguish from the van der Waals and electrostatic forces at lower Ca^{2+} concentrations (Butt *et al.* 2005). That is, with the increase in Ca^{2+} dosage, the electrostatic repulsion forces of HA with both HA and PVDF membrane decreased, whereas their hydration repulsion

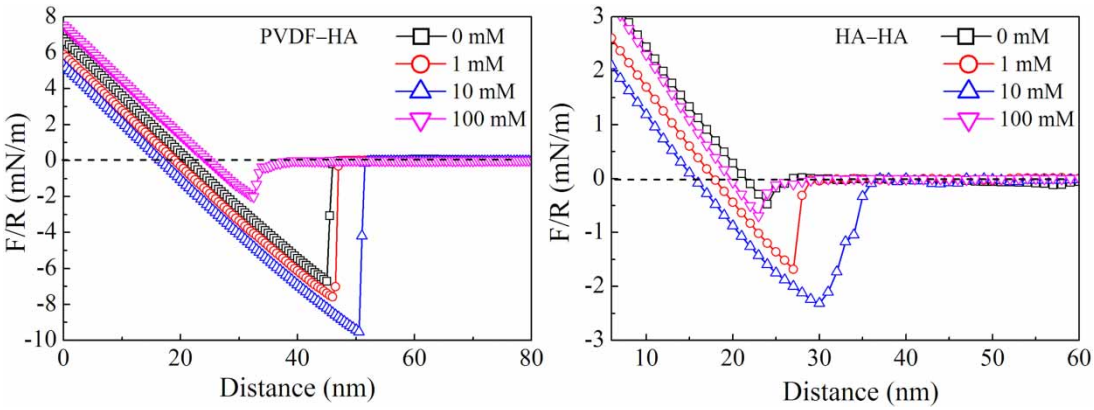

Figure 4 | The typical adhesion force curves of HA with both HA and PVDF membrane at different IS of $CaCl_2$.

forces increased (Tansel *et al.* 2006). Therefore, the balance of electrostatic interaction and hydration repulsion forces might be able to explain the variation characteristics of their corresponding adhesion force.

That is, when increasing IS from 0 to 10 mM, the increase in the adhesion forces of HA with both HA and PVDF membrane was mainly attributed to the decrease of electrostatic repulsion forces because the increase in hydration repulsion forces was weak and masked by the changes in the electrostatic forces (Israelachvili 2012). Conversely, when the IS increased to 100 mM, the amount of hydrated Ca^{2+} in the vicinity of the HA and membrane surfaces increased markedly, which resulted in a much stronger hydration repulsion force of HA with both HA and membrane (Valle-Delgado *et al.* 2011). This stronger hydration repulsion force masked the corresponding changes in the electrostatic repulsion force, which eventually led to a decline in the adhesion forces of HA–HA and HA–PVDF.

This is also the reason why the HA rejection at IS 100 mM visibly declined. The stronger hydration repulsion force could result in a higher diffusion coefficient of HA molecules; therefore, the HA with a relatively smaller size could pass more easily through the membrane and into the permeate, thus weakening the HA rejection of PVDF membranes at higher Ca^{2+} dosages (Wang *et al.* 2013a, 2013b).

Combining the above discussion about the micro-adhesion forces of HA–HA and PVDF–HA with those of macro fouling behaviors at corresponding Ca^{2+} dosages, it is easy to find that, at some range of IS of $CaCl_2$, the variation characteristics of macro membrane fouling appear to be well explained by the corresponding changes in the adhesion forces of HA–HA and PVDF–HA.

For example, when increasing the IS of $CaCl_2$ from 0 to 1 mM, the adhesion forces of HA–HA and PVDF–HA increased, which could accelerate the deposition of HA onto the membrane surface and result in a much denser fouling layer (Miao *et al.* 2017). Thus, the corresponding membrane fouling rate/extent and irreversible fouling were enhanced. In addition, when increasing the IS of $CaCl_2$ from 10 to 100 mM, the adhesion forces of HA with both HA and PVDF membrane began to decline because of the stronger hydration repulsion forces, which resulted in a great decrease in the membrane fouling rate/extent and irreversible fouling. Those observations are in line with previous viewpoints, namely, the stronger or weaker the adhesion force of the membrane–foulant and foulant–foulant, the more or less serious the irreversible fouling and flux decline rate/extent (Wang *et al.* 2013a, 2013b).

However, it is noteworthy that, when increasing the IS of $CaCl_2$ from 1 to 10 mM, the adhesion forces of HA with both HA and membrane increased with increasing Ca^{2+} dosage, whereas the irreversible fouling and flux decline rate/extent of the HA-fouled membrane declined significantly. That is, the increase in adhesion forces of HA with both HA and membrane was accompanied by less membrane fouling. This seems to suggest that, at IS of 10 mM $CaCl_2$, the changes in macro membrane fouling behavior do not appear to be fully explained by the changes of corresponding adhesion forces. In addition, the HA fouling mechanisms of membranes at different Ca^{2+} dosages were different; therefore, further studies need to analyze and resolve these issues.

Effects of Ca^{2+} concentrations on HA fouling layer structure

Based on the macro fouling experiments and the micro PVDF–HA/HA–HA adhesion forces described above, the

HA fouling layer structures on membrane surfaces at corresponding Ca^{2+} concentrations were investigated systematically by QCM-D in conjunction with self-made PVDF-coated sensor crystals. The results are presented in Figure 5. It is clear that the variation trend of the $|\Delta D/\Delta f|$ value with increasing Ca^{2+} dosage can be divided into two stages.

When increasing the IS of $CaCl_2$ from 0 to 1 mM, the $|\Delta D/\Delta f|$ value decreased rapidly from 10.6×10^{-8} to 1.4×10^{-8}, which suggests that the HA fouling layer became much denser with addition of Ca^{2+}. Combined with the results of macro membrane fouling and microadhesion forces at corresponding Ca^{2+} dosages, it is easy to find that the effects of Ca^{2+} on HA fouling behavior completely followed the Derjaguin–Landau–Verwey–Overbeek theory in this range of Ca^{2+} dosages (Israelachvili 2012). That is, with the increase in Ca^{2+} dosage, the electrostatic repulsion forces of HA–HA and PVDF–HA decreased, which accelerated the deposition of HA onto the membrane surface, and formation of a more compacted HA fouling layer finally led to a more serious membrane fouling rate and irreversible fouling.

In contrast to the observations at IS of 0–1 mM, the $|\Delta D/\Delta f|$ value increased from 1.4×10^{-8} to 5.2×10^{-8} when increasing the IS from 1 to 10 mM, which indicated that the HA fouling layer became loose and porous at an IS of 10 mM, compared with that at an IS of 1 mM. It is generally accepted that the stronger the adhesion force of HA–HA, the more compact the HA fouling layer (Wang *et al.* 2013a, 2013b). However, at an IS of 10 mM, the adhesion force of HA–HA was the strongest, whereas the HA fouling layer became looser. This phenomenon could well be explained by the aggregation of HA molecules.

As shown in Table 2, the hydrodynamic diameter of HA increased sharply from 222 nm to 768 nm when increasing the IS from 1 to 10 mM. This is mainly because

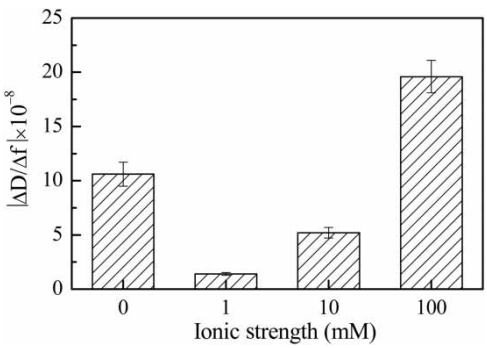

Figure 5 | The $|\Delta D/\Delta f|$ values for the HA fouling layer at various IS of $CaCl_2$.

Table 2 | Hydrodynamic diameter of HA at different Ca^{2+} dosages

Ionic strengths	0 mM	1 mM	10 mM	100 mM
Hydrodynamic diameter (nm)	212 ± 14	222 ± 23	768 ± 31	1,379 ± 108

HA is rich in carboxyl functional groups and Ca^{2+} promotes bridging between the carboxyl functional groups; i.e., two adjacent HA molecules aggregate together through their bridging actions. The aggregation phenomena of HA intensify as the Ca^{2+} dosage continues to increase, which could result in the formation of larger HA aggregates (Katsoufidou *et al.* 2005). These larger aggregates were much more difficult to pass through the membrane. As a result, it is much easier for these large HA aggregates to be retained on a membrane surface with a more porous fouling layer (Yuan & Zydney 2000). This phenomenon suggests that a pretreatment choice, such as coagulation/flocculation, which could result in the formation of larger foulant aggregates, may be an effective measure to mitigate membrane fouling.

The $|\Delta D/\Delta f|$ increased rapidly to 19.6×10^{-8} when the IS of $CaCl_2$ further increased to 100 mM, which indicated that the HA fouling layer became increasingly porous. As shown in Table 2, the hydrodynamic diameter of HA at an IS of 100 mM increased to 1,379 nm. This observation is similar to that at an IS of 10 mM, which could be explained by the aggregation phenomena of HA molecules. However, it is worth noting that the HA rejection began to decrease at an IS of 100 mM, which is different from that at an IS of 10 mM. This may be because a stronger hydration repulsion force is generated at an IS of 100 mM, which becomes another key factor in controlling the HA fouling of membrane other than the aggregates of HA molecules. The stronger hydration repulsion could effectively weaken the compactness of the HA fouling layer and the adhesion forces of HA with both HA and PVDF membrane. Meanwhile, it results in a higher diffusion coefficient of HA molecules, which causes the HA with relatively lower size to pass more easily through the membrane and into the permeate. Therefore, the HA rejection of PVDF membranes is weakened (Wang *et al.* 2013a, 2013b), which eventually leads to the fouling rate/extent and irreversible fouling of HA-fouled membrane steadily becoming weaker. It is worth noting that the decrease in membrane fouling at an IS value of 100 mM $CaCl_2$ appears to be at the cost of sacrificing HA removal efficiency. Therefore, when the hydration

repulsion force is generated, the mitigation extent of membrane fouling and the foulant rejections should be considered comprehensively in actual operation processes.

CONCLUSION

Based on the above analysis, it is easy to find that the effects of Ca^{2+} on HA fouling behavior were different for different Ca^{2+} dosages and could be divided into three stages.

When increasing the IS of $CaCl_2$ from 0 to 1 mM, membrane fouling with HA was mainly controlled by the changes of electrostatic repulsive forces, and membrane fouling rate/extent and irreversible fouling were increased with increasing Ca^{2+} dosage. This is mainly because the electrostatic repulsive forces of HA with both HA and PVDF membranes decreased with the addition of Ca^{2+} ions, which could promote the deposition of HA onto the membrane surface, and the formation of a more compacted fouling layer, eventually leading to more serious membrane fouling.

When the IS of $CaCl_2$ increased to 10 mM, the aggregates of HA molecules appeared to be the primary factor controlling membrane fouling behavior, which could cause less membrane fouling rate/extent and irreversible fouling. To be more precise, the increase in the Ca^{2+} dosage could promote the formation of large HA aggregates, which could not penetrate the membrane and will be retained on the membrane surface. This not only improved the HA rejection, but also resulted in a more porous HA fouling layer, accompanied by less membrane fouling.

When the IS of $CaCl_2$ reached 100 mM, the membrane fouling rate/extent and irreversible fouling decreased even more sharply and the HA rejection also began to decline. At this higher Ca^{2+} dosage, in addition to the aggregates of HA molecules, the hydration repulsion forces became another dominant factor controlling membrane fouling, which not only could weaken the adhesion forces of HA with both HA and PVDF membrane, but also caused the HA with relatively smaller size to pass more easily through the membrane and into the permeate, thus leading to less membrane fouling and a lower HA rejection.

ACKNOWLEDGEMENTS

We thank the Innovative Research Team of Shaanxi Province (2017KCT-19-01), the Hong Kong Scholars Program (XJ2017037), the National Natural Science Foundation of China (51608429), the Natural Science Foundation of Shaanxi Province (2016JQ5067), the Educational Commission of Shaanxi Province of China (16JS062), the key industrial chain (group) project of Shaanxi Province (2017ZDCXL-GY-07-01), and the Postdoctoral Science Foundation of Shaanxi Province for the support of this research.

REFERENCES

Butt, H. J., Cappella, B. & Kappl, M. 2005 Force measurements with the atomic force microscope: technique, interpretation and applications. *Surface Science Reports* **59** (1), 1–152.

Chang, X. & Bouchard, D. C. 2013 Multiwalled carbon nanotube deposition on model environmental surfaces. *Environmental Science & Technology* **47** (18), 10372–10380.

Israelachvili, J. N. 2012 *Intermolecular and Surface Forces,* revised 3rd edn. Academic Press, London.

Katsoufidou, K., Yiantsios, S. G. & Karabelas, A. J. 2005 A study of ultrafiltration membrane fouling by humic acids and flux recovery by backwashing: experiments and modeling. *Journal of Membrane Science* **266** (1), 40–50.

Katsoufidou, K., Yiantsios, S. G. & Karabelas, A. J. 2008 An experimental study of UF membrane fouling by humic acid and sodium alginate solutions: the effect of backwashing on flux recovery. *Desalination* **220** (1–3), 214–227.

Kyzas, G. Z., Bikiaris, D. N. & Lambropoulou, D. A. 2017 Effect of humic acid on pharmaceuticals adsorption using sulfonic acid grafted chitosan. *Journal of Molecular Liquids* **230**, 1–5.

Lin, T., Lu, Z. & Chen, W. 2015 Interaction mechanisms of humic acid combined with calcium ions on membrane fouling at different conditions in an ultrafiltration system. *Desalination* **357**, 26–35.

Miao, R., Wang, L., Gao, Z., Mi, N., Liu, T., Lv, Y. & Wang, X. 2015 Polyvinylidene fluoride/poly(ethylene-co-vinyl alcohol) blended membranes and a systematic insight into their antifouling properties. *RSC Advances* **5** (46), 36325–36333.

Miao, R., Wang, L., Deng, D., Li, S., Wang, J., Liu, T., Zhu, M. & Lv, Y. 2017 Evaluating the effects of sodium and magnesium on the interaction processes of humic acid and ultrafiltration membrane surfaces. *Journal of Membrane Science* **526**, 131–137.

Mo, H., Tay, K. G. & Ng, H. Y. 2008 Fouling of reverse osmosis membrane by protein (BSA): effects of pH, calcium, magnesium, ionic strength and temperature. *Journal of Membrane Science* **315** (1), 28–35.

Nghiem, L. D., Oschmann, N. & Schäfer, A. I. 2006 Fouling in greywater recycling by direct ultrafiltration. *Desalination* **187** (1–3), 283–290.

Nghiem, L. D., Vogel, D. & Khan, S. 2008 Characterising humic acid fouling of nanofiltration membranes using bisphenol A as a molecular indicator. *Water Research* **42** (15), 4049–4058.

Seidel, A. & Elimelech, M. 2002 Coupling between chemical and physical interactions in natural organic matter (NOM) fouling of nanofiltration membranes: implications for fouling control. *Journal of Membrane Science* **203** (1), 245–255.

Shankar, V., Heo, J., Al-Hamadani, Y. A., Park, C. M., Chu, K. H. & Yoon, Y. 2017 Evaluation of biochar-ultrafiltration membrane processes for humic acid removal under various hydrodynamic, pH, ionic strength, and pressure conditions. *Journal of Environmental Management* **197**, 610–618.

Shao, J., Hou, J. & Song, H. 2011 Comparison of humic acid rejection and flux decline during filtration with negatively charged and uncharged ultrafiltration membranes. *Water Research* **45** (2), 473–482.

Shen, Y., Kim, H., Tong, M. & Li, Q. 2011 Influence of solution chemistry on the deposition and detachment kinetics of RNA on silica surfaces. *Colloids and Surfaces B: Biointerfaces* **82** (2), 443–449.

Singh, G. & Song, L. 2005 Quantifying the effect of ionic strength on colloidal fouling potential in membrane filtration. *Journal of Colloid and Interface Science* **284** (2), 630–638.

Sutzkover-Gutman, I., Hasson, D. & Semiat, R. 2010 Humic substances fouling in ultrafiltration processes. *Desalination* **261** (3), 218–231.

Szymański, K., Morawski, A. W. & Mozia, S. 2016 Humic acids removal in a photocatalytic membrane reactor with a ceramic UF membrane. *Chemical Engineering Journal* **305**, 19–27.

Tang, C. Y., Kwon, Y. N. & Leckie, J. O. 2007 Characterization of humic acid fouled reverse osmosis and nanofiltration membranes by transmission electron microscopy and streaming potential measurements. *Environmental Science & Technology* **41** (3), 942–949.

Tansel, B., Sager, J., Rector, T., Garland, J., Strayer, R. F., Levine, L. & Bauer, J. 2006 Significance of hydrated radius and hydration shells on ionic permeability during nanofiltration in dead end and cross flow modes. *Separation and Purification Technology* **51** (1), 40–47.

Tian, J. Y., Ernst, M., Cui, F. & Jekel, M. 2013 Effect of different cations on UF membrane fouling by NOM fractions. *Chemical Engineering Journal* **223**, 547–555.

Valle-Delgado, J. J., Molina-Bolívar, J. A., Galisteo-González, F. & Gálvez-Ruiz, M. J. 2011 Evidence of hydration forces between proteins. *Current Opinion in Colloid & Interface Science* **16** (6), 572–578.

Wang, L., Miao, R., Wang, X., Lv, Y., Meng, X., Yang, Y. & Ju, K. 2013a Fouling behavior of typical organic foulants in polyvinylidene fluoride ultrafiltration membranes: characterization from microforces. *Environmental Science & Technology* **47** (8), 3708–3714.

Wang, L. L., Wang, L. F., Ye, X. D. & Yu, H. Q. 2013b Hydration interactions and stability of soluble microbial products in aqueous solutions. *Water Research* **47** (15), 5921–5929.

Wang, L. F., He, D. Q., Chen, W. & Yu, H. Q. 2015 Probing the roles of Ca^{2+} and Mg^{2+} in humic acids-induced ultrafiltration membrane fouling using an integrated approach. *Water Research* **81**, 325–332.

Yamamura, H., Kimura, K., Okajima, T., Tokumoto, H. & Watanabe, Y. 2008 Affinity of functional groups for membrane surfaces: implications for physically irreversible fouling. *Environmental Science & Technology* **42** (14), 5310–5315.

Yuan, W. & Zydney, A. L. 1999 Effects of solution environment on humic acid fouling during microfiltration. *Desalination* **122** (1), 63–76.

Yuan, W. & Zydney, A. L. 2000 Humic acid fouling during ultrafiltration. *Environmental Science & Technology* **34** (23), 5043–5050.

First received 19 October 2017; accepted in revised form 14 March 2018. Available online 28 March 2018